EOS Imaging

**Alessandro De Leucio, Estelle Tenisch,
Pierre Yves Zambelli, and Patrick Omoumi**

Introduction

The EOS system is an X-ray system that allows to obtain high-quality whole-body radiograms with a much lower dose than conventional radiography in a standing or sitting position.

*A. De Leucio and E. Tenisch contributed equally.

—————

A. De Leucio (✉)
Department of Radiology, Reine Fabiola University Children's Hospital, Brussels, Belgium
e-mail: alessandro.deleucio@huderf.be

E. Tenisch · P. Omoumi
Department of Diagnostic and Interventional Radiology, Lausanne University Hospital, Lausanne, Switzerland
e-mail: estelle.tenisch@chuv.ch

P. Y. Zambelli
Division of Pediatric Orthopedics, Department Women-mother-child, Lausanne University Hospital, Lausanne, Switzerland

The technological key element of the EOS system is the multi-wire proportional chamber, for which Georges Charpak was awarded the Nobel Prize in 1992.

The high efficiency of the "Charpak chamber" to capture photons permits drastically lower milliampere (mA) values of the X-ray beam compared to traditional radiographic systems, resulting in high-quality diagnostic images obtained at very low doses [1–3].

Another significant technical element of EOS imaging is the very thinly collimated X-ray beam, which results almost parallel. Conventional radiographic systems use a conical X-ray beam that delivers a higher dose to the patient and induces the well-known magnification artifact for the structures far from the center of the image. The highly collimated parallel X-ray beam of the EOS system allows to reduce the dose and encounters only limited deformations of the images without magnification. Thus, EOS imaging is particularly suitable to obtain a 3D reconstruction of the spine and lower limb bony structures by stereoradiography [2, 4].

The EOS imaging system is composed of two X-ray tubes and two "Charpak's chambers," which move synchronously on the vertical axis, allowing the simultaneous acquisition of frontal and lateral images of the whole body. The possibility of obtaining images of the whole body and in a natural standing position makes the EOS system an excellent tool for studying pathologies of the spine, lower limbs, and pelvis in children and adults [3, 4].

The very low dose delivered to the patient is a highly valued element in pediatric radiology [1, 3].

After the acquisition, the EOS image undergoes advanced post-processing through the SterEOS® software [1, 2, 4].

SterEOS post-processing allows users to obtain a large number of measurements of medical interest automatically (whether scalar, vector, or angular) of the spine, pelvis, and lower limbs, in both a two-dimensional (2D) and three-dimensional (3D) way.

The EOS system is used for studying many pathologies of the lower limbs. EOS imaging allows an accurate assessment

of lower limb length discrepancy, the deformation in varus or valgus, and many other pathologies, as well as being helpful for preoperative planning.

Usually, children can take the exam from the age when they can stand alone in the imaging system booth without moving for 40 s (generally from 7 years old in our experience).

Spine and Pelvis

Whenever available, low-dose radiography using EOS has replaced standard radiographs for the quantitative assessment of the spine and pelvis in children.

The following are a set of measurements routinely performed in clinical practice. The measurements may be performed using the SterEOS application or manually, using the software available on the PACS (Picture Archiving And Communication System).

Pelvic Measurements

Pelvic measurements are essential as the position of the pelvis determines the position of the lumbar spine and thereby of the entire spine. EOS imaging delivers a dose 2.4 inferior to conventional radiography when imaging the pelvis [5].

Pelvic Incidence (PI)

On the lateral view, the pelvic incidence (PI) is defined as the angle between two lines:

1. A line between the center of the femoral heads and the center of S1 endplate (if the femoral heads are not perfectly superposed on the lateral view, the reference point lies midway between the centers of the two femoral heads).
2. A line perpendicular to a line tangent to the endplate of S1.

The PI remains constant after skeletal maturity and does not change with the patient position. Pelvic incidence is the fundamental pelvic parameter in the three-dimensional development of the sagittal curves of the spine. Based on the PI value, the geometry of the physiological lumbar lordosis can be theoretically predicted [6].

The lower the PI, the narrower the pelvis (as measured in the anteroposterior axis). The greater the PI, the wider the pelvis. The PI increases slightly with age, following the onset of unassisted bipedal locomotion in children.

Normal values [7]:

- 44.0 ± 6.5 degrees in children between 2 and 9 years old.
- 48.1 ± 8.5 degrees in children between 10 and 15 years old.
- 46.6 ± 8.4 degrees in children between 15 and 20 years old (Fig. 1).

Sacral Slope (SS)

The sacral slope (SS) is defined as the angle between:

1. The horizontal plane.
2. The axis of S1 endplate.

The value of the SS may vary depending on the patient's position.

Hence, a horizontal pelvis has a greater SS and a vertically oriented pelvis has a lower SS value. The SS remains relatively unchanged during growth. Sagittal sacro-pelvic alignment is most commonly assessed in children from the pelvic tilt (PT) and the sacral slope (SS), i.e. PI=SS + PT.

Normal values [8]:

- Between 3 and 8 years old: 38.2 ± 7.7 °.
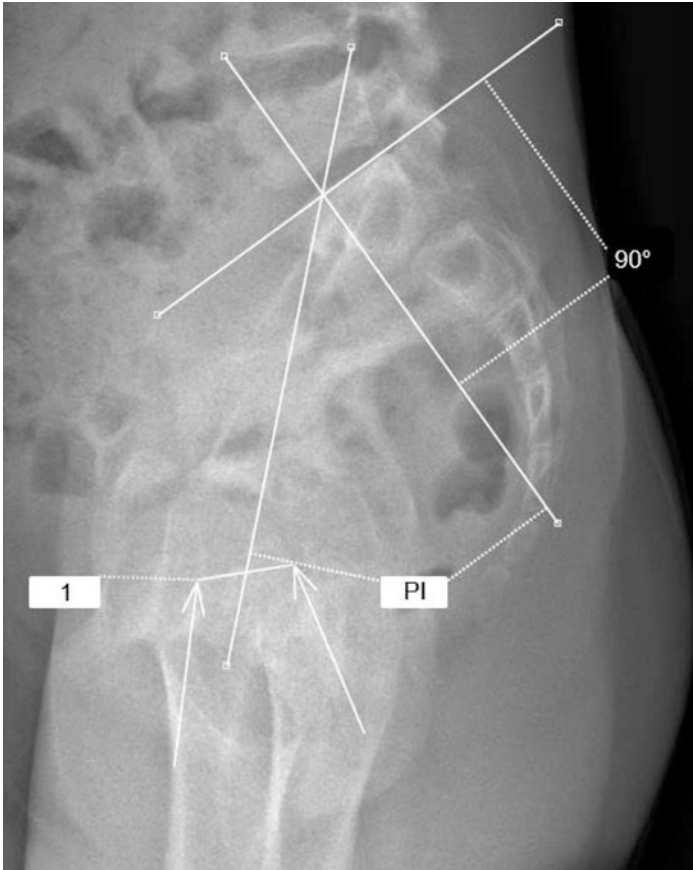- Between 8 and 18 years old: 39.1 ± 7.6 ° (Fig. 2).

FIGURE 1 Pelvic incidence. *1* line between the centers of the femoral heads (arrows), *PI* pelvic incidence

Pelvic Tilt (PT)

The pelvic tilt (PT) is defined as the angle between two lines:

1. The vertical plane passing through the center of the femoral heads.
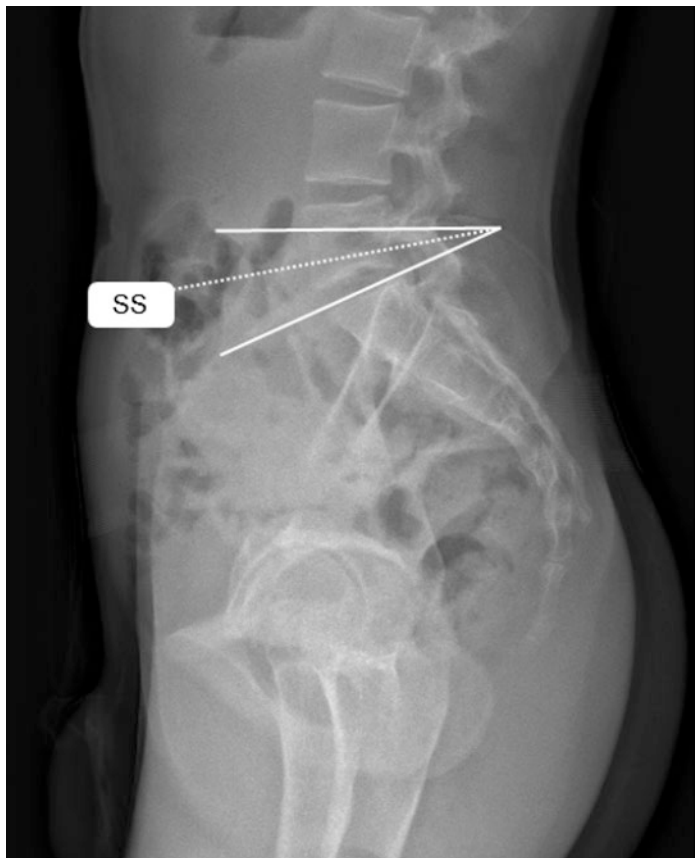2. The line between the center of the superior endplate of S1 and the center of the femoral heads.

Figure 2 Sacral slope

If the femoral heads are not perfectly superimposed, the reference point is set midway between the lines connecting the center of the femoral heads.

The value of the PT may vary depending on the patient's position.

Normal values [8]:

- Between 3 and 8 years old: $5.5 \pm 7.6\,°$.
- Between 8 and 18 years old: $7.7 \pm 8.3\,°$ (Fig. 3).

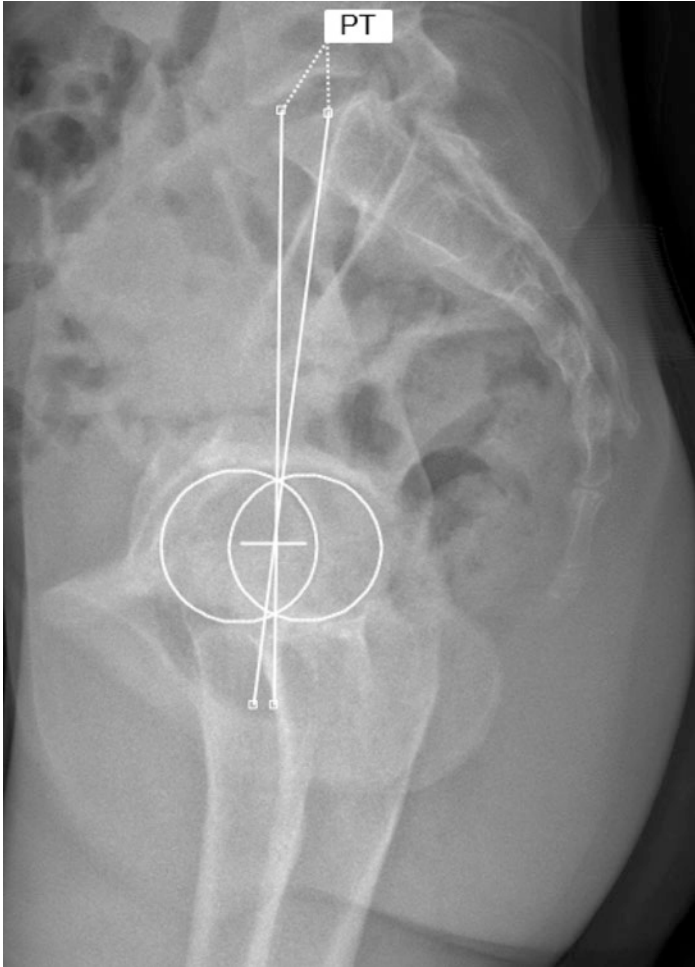Figure 3 Pelvic tilt

Pelvic Obliquity (PO)

On the coronal images of the pelvis, the pelvic obliquity corresponds to the rotation of the pelvis in the coronal plane. It is the distance between two lines (measured on a line perpendicular to lines 1 and 2):

• Line 1 drawn horizontally across the most superior aspect of one acetabulum.
• Line 2 drawn horizontally across the most superior aspect of the other acetabulum.

Abnormal PO may have supra-pelvic causes such as scoliosis or infra-pelvic causes such as hip contracture, limb amputation (with prosthesis), and lower limb length discrepancy [9] (Fig. 4).
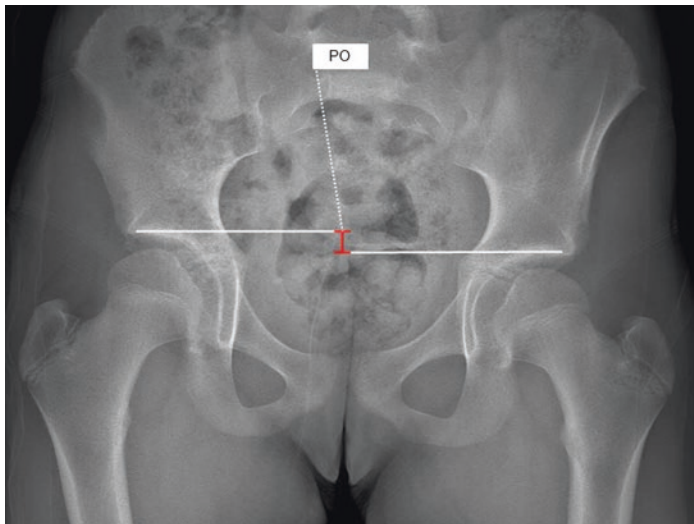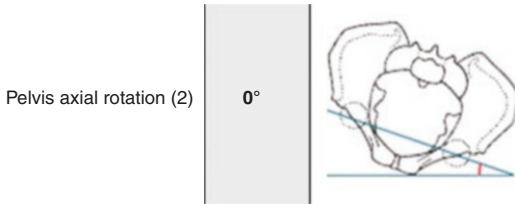

FIGURE 4 Pelvic obliquity

Figure 5 Example of the axial rotation of the pelvis as provided by the SterEOS report

Axial Rotation of the Pelvis (ARP)

The axial rotation of the pelvis is measured on 3D reconstruction and defined according to the coronal plane and measured between two lines:

1. The radiologic frontal plane (defined by the EOS acquisition planes).
2. The line between the centers of the two acetabula.

This measurement may be performed using the SterEOS® system [10] (Fig. 5).

Spine Measurements

Vertebral Numbering

When describing a spinal deformity, it is essential to use a consistent method for vertebral numbering. Cervical vertebrae are seldom involved in spinal deformities. By definition, a thoracic vertebra is associated with the presence of ribs [11]. However, radiologically, a very small rib cannot be

distinguished from a small transverse process. Moreover, normal variants such as extra pairs of ribs exist. Therefore, it is sometimes impossible to number spinal vertebrae accurately, in which case an arbitrary choice is made and must be clearly mentioned in the report. Care must also be taken to always use the same numbering as in previous examinations [11].

Coronal Balance

Coronal balance is evaluated by measuring the distance between two lines, the CSVL (central sacral vertical line) and the C7 plumb line, as follows:

1. C7 plumb line: is drawn vertically from the central point of C7 downward.
2. CSVL: is drawn vertically from the central point of S1 upward.
   The coronal balance is mainly performed to assess spinal deviation in adolescent idiopathic scoliosis. Idiopathic scoliosis generally has a right curvature, and a left curve should be evaluated by MR to assess potential underlying issues.

### C7-Central Sacral Line (CSL)

The C7-central sacral line (CSL) is the distance between two lines in the frontal plane:

1. A vertical line drawn from the central point of C7 (C7 plumb line).
2. A line drawn vertically from the central point of S1 upward (CSVL).

   Balance is abnormal if the CSL is greater than 2 cm.
   A negative value is measured when the vertical plumb line deviates to the left; a positive value is measured when the vertical plumb line deviates to the right (Fig. 6).

FIGURE 6 C7-central sacral line
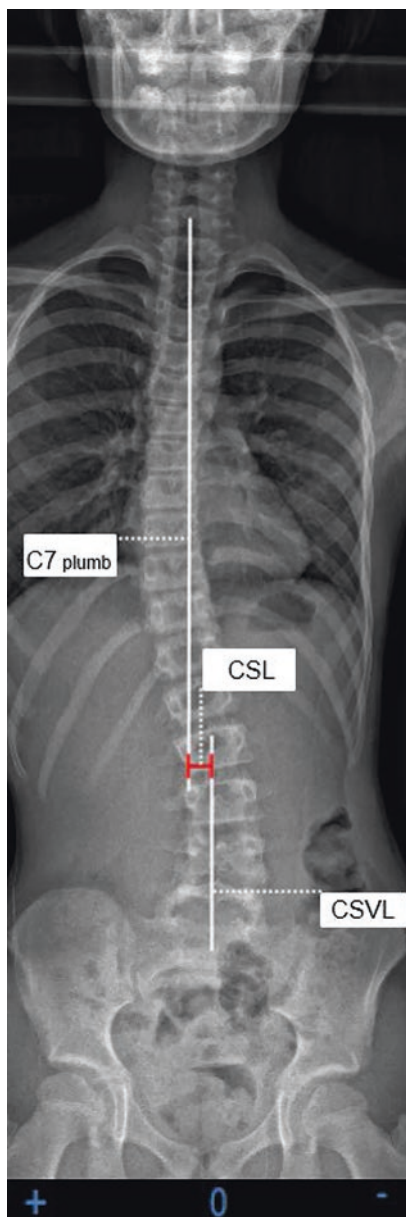
Cobb Angle

The Cobb angle is defined as the angle between the two tangents drawn along the superior endplate of the superior end vertebra and the inferior endplate of the inferior end vertebra, in the scoliotic curve. The superior or inferior borders of the pedicles can be used instead of the endplates if these are not clearly visible.

The end vertebrae are those most tilted. The apex of the curve is the disk or the vertebra most horizontal and laterally placed from the center of the vertebral column (Figs. 7 and 8).

Scoliosis is defined as a lateral spinal curvature with a Cobb angle of $\geq 10°$.

Diurnal variations of the Cobb angle up to $5°$ are possible [12].

A progressive curve that requires management is defined by a Cobb angle increase of $5°$ or more between consecutive radiographic examinations. The same measurements (same vertebrae) should be used for the follow-up examinations [12].

Structural curves, described by their location, lack normal flexibility and are termed as major (if they have the largest Cobb measurement) or minor. Minor curves can be structural or nonstructural [13]. Pelvic obliquity >2 cm must be corrected to measure the Cobb angles [13].
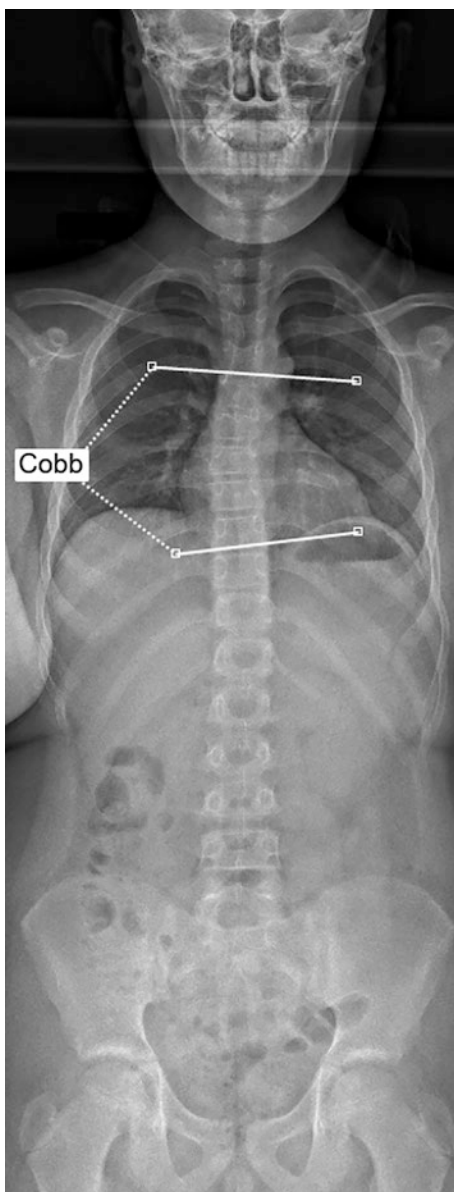
Lateral Flexion (Bending) Radiographs

If a curve cannot be corrected with ipsilateral bending to a curve <25° and/or kyphosis >20°, it is considered structural [13].

In-Brace Measurements

The measurements performed in brace should evaluate the curvature corrected by the brace with the same reference vertebrae as the image without brace.
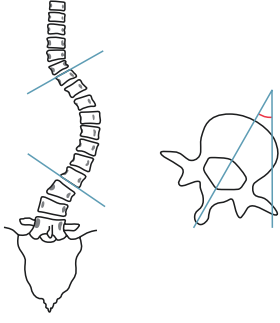
FIGURE 7 Cobb angle

Scoliosis parameters (1)		Value	
Curve (T7-T9-T12)	Cobb (T7-T9-T12)	**46°**	
	Axial rotation of apical vertebra T9	**-2°**	
Curve (T12-L1-L4)	Cobb (T12-L1-L4)	**40°**	
	Axial rotation of apical vertebra L1	**21°**	

FIGURE 8 Example of spine measurements of the Cobb angles in a SterEOS report

If the curvature of the spine increases by more than 5° during brace treatment or if it is over 40° at skeletal maturity, the diagnosis of bracing failure is made [14].

In-brace correction <25% is a predictive factor of brace treatment failure in patients with double curves [14].

Sagittal Balance

Sagittal Vertical Axis (SVA) and CAM Plumb Line

On the sagittal view, C7 plumb line is a vertical line drawn downward from the central point of the C7 vertebral body. The C7 plumb line is the reference to measure the sagittal vertical axis (SVA). The SVA is evaluated by measuring the distance between the posterosuperior aspect of the S1 vertebral body and C7 plumb line. A positive SVA is defined by a C7 plumb line anterior to the posterosuperior margin of S1 and a negative sagittal balance by a C7 plumb line posterior to the posterosuperior margin of S1. A distance >2 cm is con-

sidered abnormal. C7 plumb line tends to move backward from childhood to adulthood. Progressive forward displacement of C7 plumb line in children should raise a suspicion for the risk of spinal pathology [8].

The Center of Acoustic Meati (CAM) is defined by the distance between the vertical line drawn from the center of acoustic meati (CAM plumb line) and the center of acetabula. The CAM is positive if the CAM plumb line is anterior to the acetabula. The CAM plumb line is useful for the clinical and radiological evaluation of the sagittal balance, even if it does not coincide with the gravity line. Normative CAM values in children have not been established yet [15] (Fig. 9).
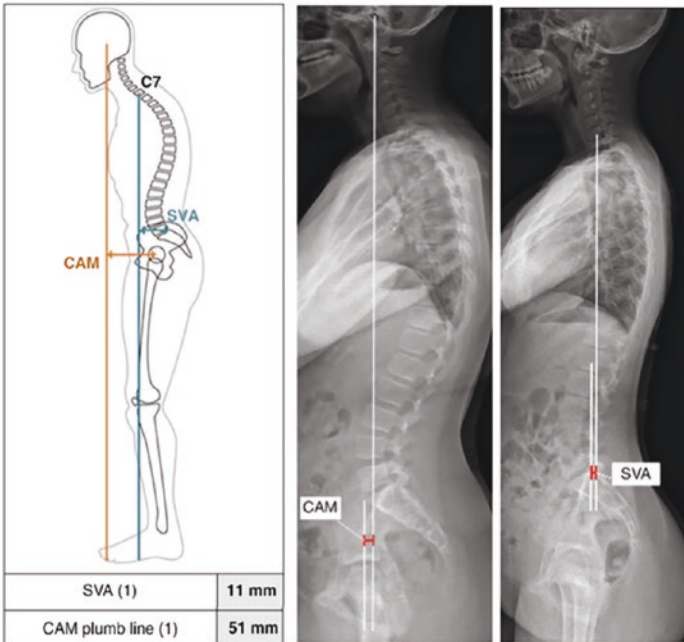

FIGURE 9 Example of SVA and CAM plumb line provided in a SterEOS report

Spino-Sacral Angle (SSA)

The spino-sacral angle (SSA) corresponds to an angle measured between two lines:

• A line drawn from the central point of C7 to the midpoint of the superior endplate of S1.
• A line tangent to the endplate of S1.

Normal SSA values are 130° ± 10° in subjects aged 3–10 years and 133° ± 8° in subjects between 10 and 18 years [8] (Fig. 10).

| Spino Sacral Angle (1) | **128°** |
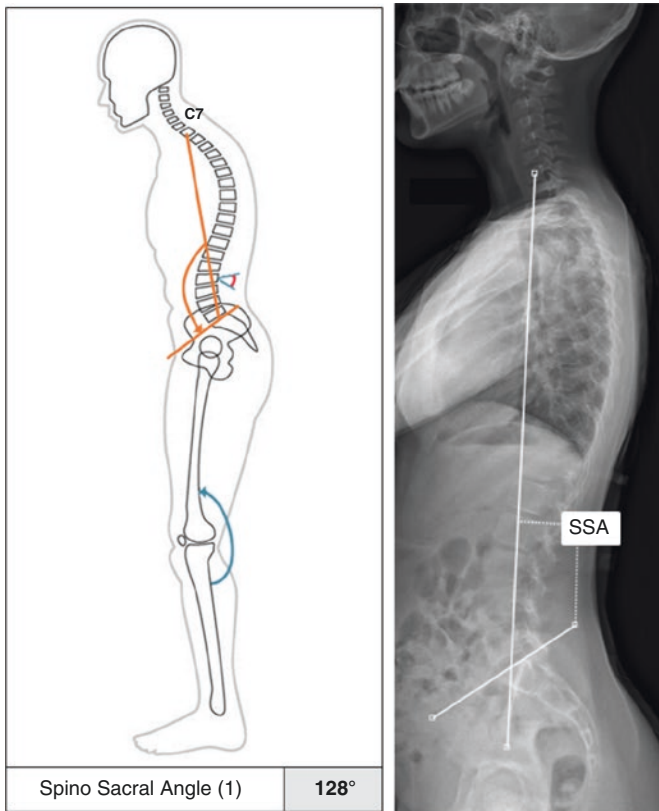
Figure 10 Example of SSA provided in a SterEOS report

T9 Tilt or T9 Sagittal Offset

In the sagittal plane, the T9 tilt (also know as Duval-Beaupère angle) is the angle formed by two lines (Fig. 11):

– A line between the central point of the two femoral heads and the central point of T9.
– A vertical line drawn upward from the central point of the two femoral heads.

This angle is positive when the hip axis lies in front of the T9 vertebral center. There are no published values for children. However, its normal value is 11.3 ± 3.52 in young adults and it is considered relatively stable during life [16, 17].

Thoracic Kyphosis (TK) and Lumbar Lordosis (LL)

The thoracic kyphosis (TK) and lumbar lordosis (LL) are measured by Cobb angles (Fig. 12). By convention, kyphosis is a positive (+) measurement and lordosis is a negative (−) measurement.

The TK is the angle measured between the superior endplate of T1 and the inferior endplate of T12. Its theoretical value is 0.75 x L1-S1 lordosis. T1–T4 represents only 8–10° of the overall kyphosis. For this reason, when it is impossible to visualize properly the first thoracic vertebra, it is acceptable to measure the TK between T5 and T12. Normal values are comprised between 10° and 40°.

The LL is the angle measured between the superior endplate of L1 and the inferior endplate of L5.

When operating a scoliosis, the most important thing for the surgeon is to preserve the sagittal balance. After spine fixation, one of the major complications is the junctional syndrome, occurring generally in the first months after surgery. It is defined as an increase in the proximal kyphosis of $\geq 10°$, which is the angle measured between the inferior endplate of the first instrumented vertebra and the superior endplate of the second vertebra above it [18, 19].

3D Images

An added advantage offered by the EOS compared to conventional radiographs is to allow 3D analysis (Figs. 11, 12, and 13).
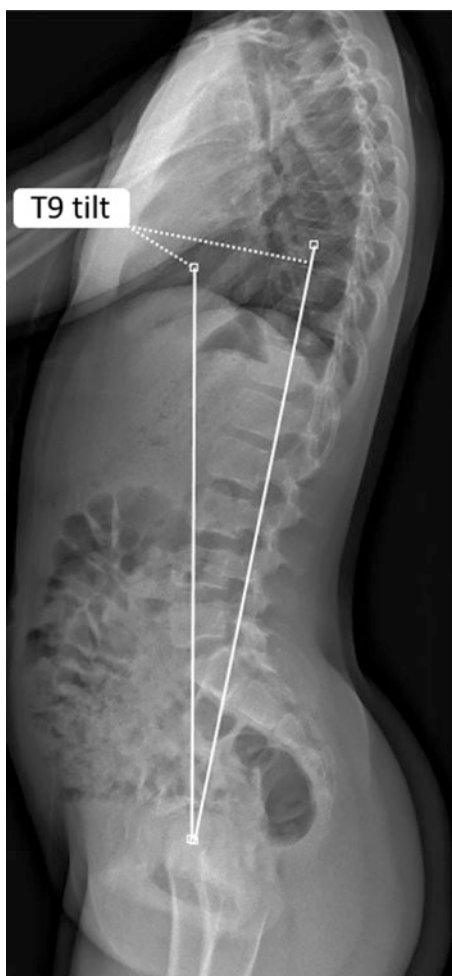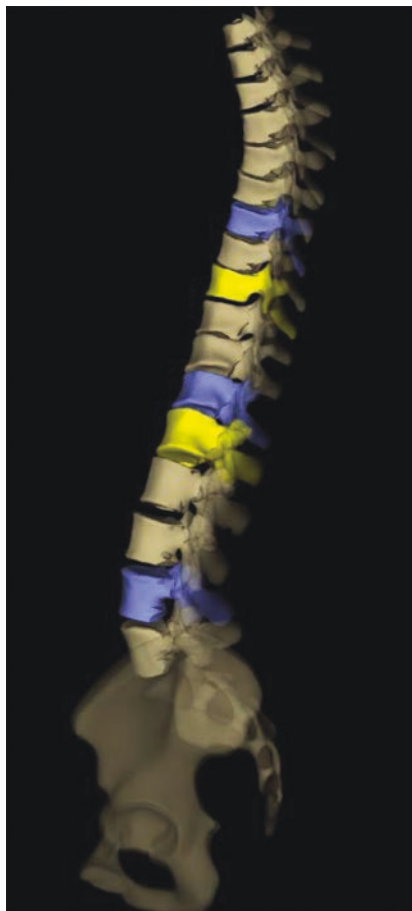

Figure 11 T9 tilt

Figure 12 Thoracic
kyphosis and lumbar
lordosis

FIGURE 13 Example of a spine 3D reconstruction provided in a SterEOS report (lateral view)

Measurements of pelvic position were shown to be accurate and reliable with EOS. Reconstructed 3D images are within 1.1 mm ($\mp$ 0.2 mm) when compared to CT scan images. However, because these 3D reconstructions are based on standard bone models, they cannot be performed in cases of vertebral malformations, and they are not suitable for analyzing the ossification of the iliac apophysis (Risser classification) [20, 21] (Figs. 14 and 15).
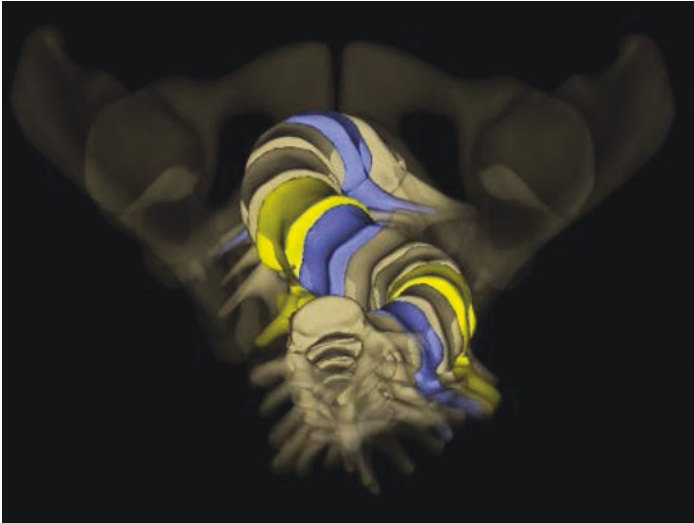
FIGURE 14 Example of a spine 3D reconstruction provided in a SterEOS report (cranio-caudal view)
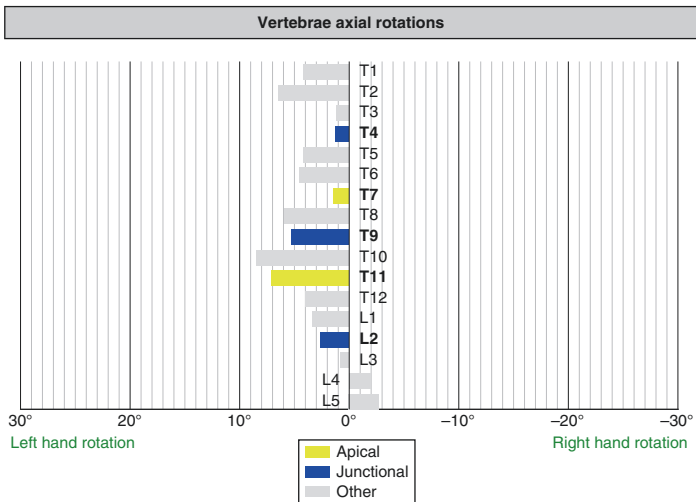

FIGURE 15 The diagram provides the axial rotation of the vertebrae calculated in relation to the pelvis

Lower Limb Measurements

Due to the relative novelty of the EOS imaging, few studies are currently available on the lower limb anatomical parameters in normal pediatric individuals. In this section, 16 lower limb measurements derived from EOS imaging are described.

1. Femoral Mechanical Axis Length [cm]: distance between the central point of the femoral head (A) and the midpoint of the distal femoral joint surface (B) (Figs. 16 and 17).

2. Tibial Mechanical Axis Length [cm]*: the distance between the midpoint of the intercondylar eminence (point C) and the midpoint of the distal tibial surface at the ankle (point D) (Fig. 17).

Age group (in years)	MALE	FEMALE
4 - 6	27.0 ± 2.0	25.5 ± 2.8
7 - 8	30.7 ± 2.9	30.6 ± 2.2
9 - 10	35.2 ± 2.2	35.9 ± 2.7
11 - 12	39.2 ± 3.0	39.6 ± 2.5
13 - 14	43.2 ± 2.2	40.9 ± 2.4
15 - 16	43.7 ± 2.5	41.2 ± 2.2

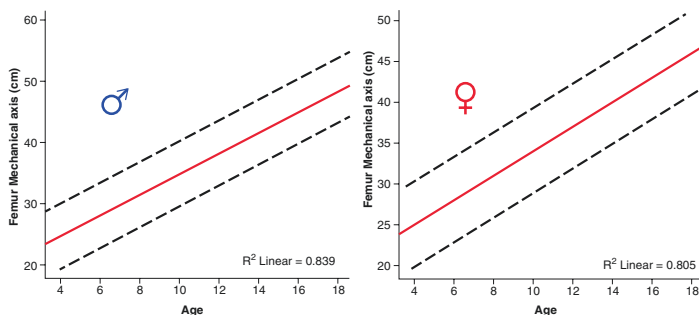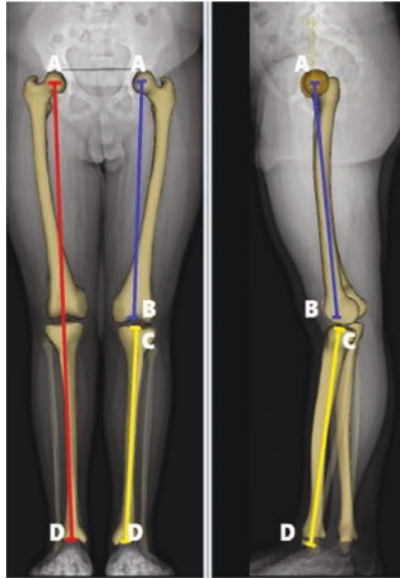
FIGURE 16 Adapted from Szuper et al. [22]

FIGURE 17 Lower
limb axis

3. Functional Length of the Lower Limb [cm]*: the distance between points A and D (Fig. 17).
4. Anatomical Length of the Lower Limb [cm]*: the sum of the distance AB + CD (Fig. 17).
*At the time of writing, there are no published EOS imaging studies on the parameters described in points 2, 3 and 4.
5. Femoral Head Diameter [mm] (Fig. 18):
6. Femoral Offset [mm]: the distance between the central point of the femoral head and the line drawn through the femoral diaphysis axis are presented in the table below and in Fig. 19 (red line).

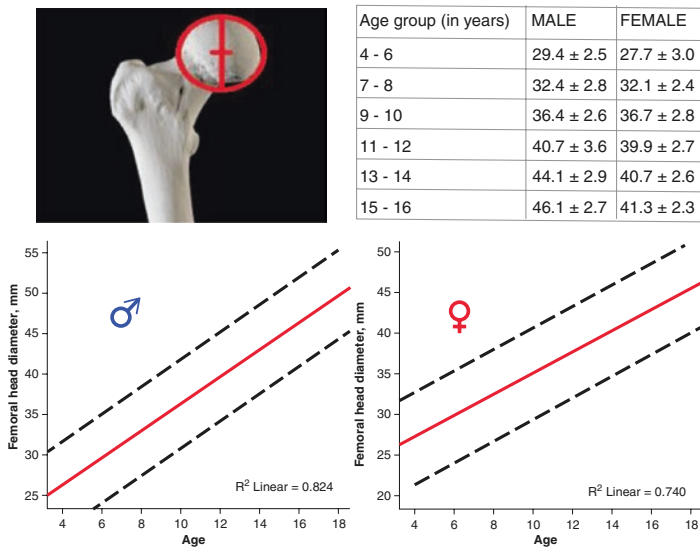| Age group (in years)	MALE	FEMALE
4 - 6	29.4 ± 2.5	27.7 ± 3.0
7 - 8	32.4 ± 2.8	32.1 ± 2.4
9 - 10	36.4 ± 2.6	36.7 ± 2.8
11 - 12	40.7 ± 3.6	39.9 ± 2.7
13 - 14	44.1 ± 2.9	40.7 ± 2.6
15 - 16	46.1 ± 2.7	41.3 ± 2.3

FIGURE 18 Adapted from Szuper et al. [22]

7. Femoral Neck Length [mm]: distance measured between the central point of the femoral head and the line bisecting the proximal femoral diaphysis (Fig. 20) (red line).

8. Neck/Shaft Angle (NSA) [Degrees]: the angle between the axis of the femoral diaphysis and the axis of the femoral neck originating from the center of the femoral head on the frontal plane (Fig. 21).

9. Femoral Mechanical Angle (FMA) [Degrees]: the angle between the femoral mechanical axis and the posterior bicondylar tangential line of the femur (Fig. 22).

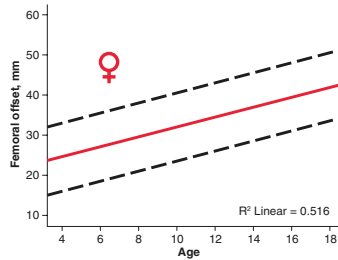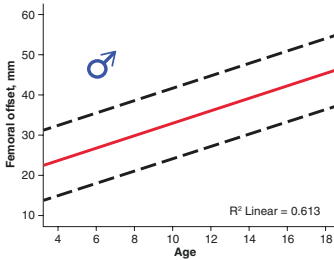| Age group (in years)	MALE	FEMALE
4 - 6	26.8 ± 3.8	25.5 ± 3.6
7 - 8	29.1 ± 3.4	29.0 ± 4.0
9 - 10	32.6 ± 4.2	32.5 ± 4.2
11 - 12	37.4 ± 4.5	36.8 ± 4.3
13 - 14	39.8 ± 4.7	37.5 ± 4.6
15 - 16	42.4 ± 4.9	37.9 ± 3.8

FIGURE 19   Adapted from Szuper et al. [22]

10. Tibial Mechanical Angle (TMA) [Degrees]: the angle between the tibial mechanical axis and the posterior bicondylar tangential line of the tibia (Fig. 23).

11. Mechanical Tibiofemoral Angle (FTA) [Degrees]: angle between the femoral and the tibial mechanical axis on the frontal plane. The varus and valgus deformation values of the knee are derived from this angle using the formula (180 °−FTA). Negative values mean varus, while positive values indicate valgus deformation (Fig. 24).

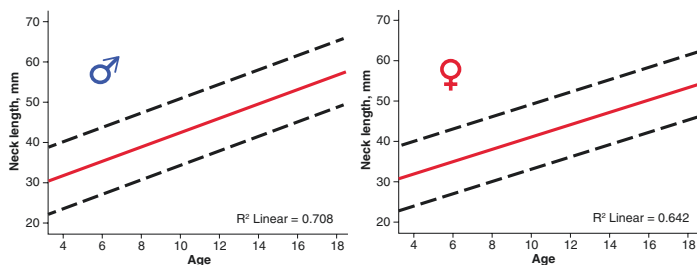| Age group (in years)	MALE	FEMALE
4 - 6	35.0 ± 4.0	32.8 ± 3.2
7 - 8	37.9 ± 3.4	37.2 ± 3.3
9 - 10	42.8 ± 3.3	42.9 ± 4.2
11 - 12	47.3 ± 4.3	46.8 ± 4.1
13 - 14	50.7 ± 4.1	48.2 ± 3.9
15 - 16	52.9 ± 4.3	48.1 ± 3.5

FIGURE 20   Adapted from Szuper et al. [22]

12. Hip-Knee-Shaft Angle (HKS) [Degrees]: angle between the mechanical femoral axis and the axis of the distal diaphysis on the frontal plane (Fig. 25).
13. Femoral Torsion Angle (FT) or Femoral Anteversion [Degrees]: angle defined between the femoral neck axis and the posterior bicondylar tangential line of the femur when projected on a plane orthogonal to the mechanical axis of the femur.

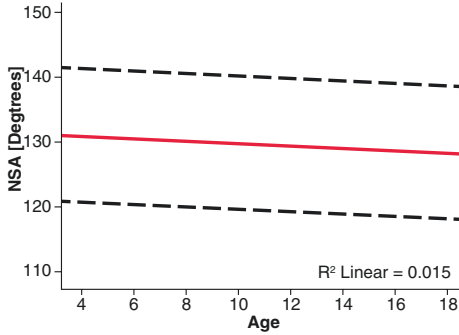| Age group (in years)	
4 - 6	130.4 ± 4.9
7 - 8	130.1 ± 5.3
9 - 10	130.9 ± 6.2
11 - 12	128.7 ± 4.5
13 - 14	129.2 ± 5.0
15 - 16	127.9 ± 4.3

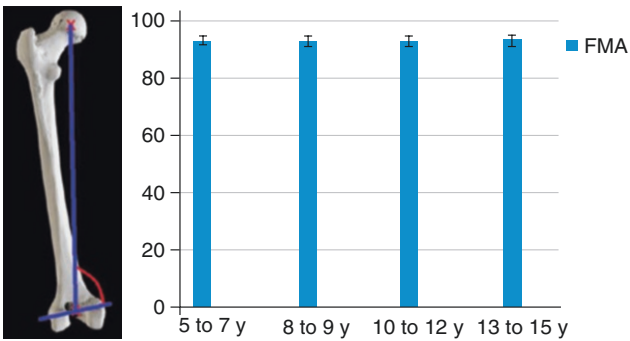FIGURE 21 Adapted from Szuper et al. [22]

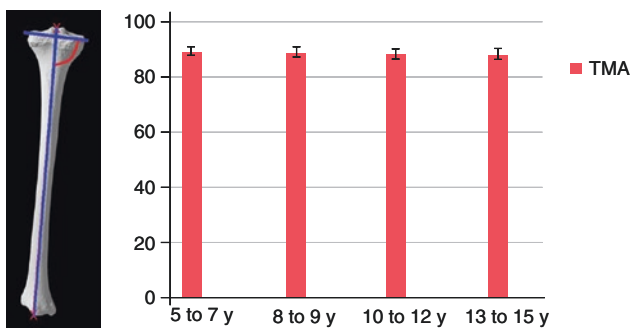FIGURE 22 Adapted from Rampal et al. [23]
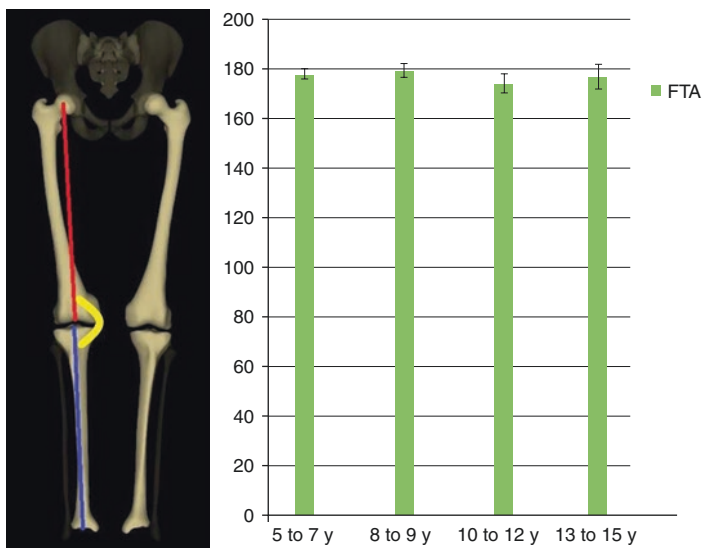
FIGURE 23 Adapted from Rampal et al. [23]

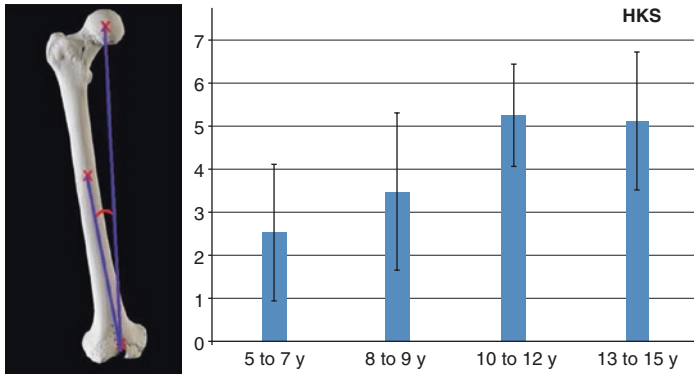FIGURE 24 Adapted from Rampal et al. [23]

FIGURE 25 Adapted from Rampal et al. [23]

The FT is specific to the bipedal position of humans [24]. In humans, there is an early femoral torsion followed by a slow derotation that progresses throughout growth until adulthood (Fig. 26).

- The FT rapidly increases during the intrauterine life from the fourth to the ninth month. At birth, the FT is between 35° and 41° [25, 26].
- Later the distal femur tends to progressively rotate outward, and this angle decreases to the values described in Fig. 26.
- In adults, the normal value is 15.6 ± 6.7° [27].

14. Tibial Torsion Angle (TT) [Degrees]: angle defined between the posterior bicondylar tangential line of the tibia and the transmalleolar axis when projected on a plane orthogonal to the tibial mechanical axis.

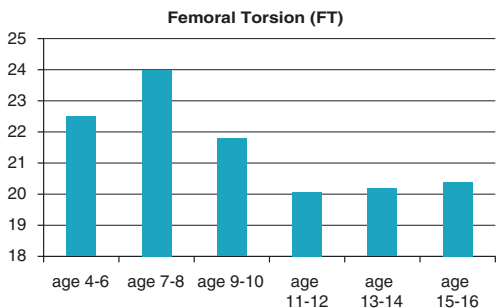This angle is usually positive in children, so the two malleoli are rotated relative to the tibia (Fig. 27).
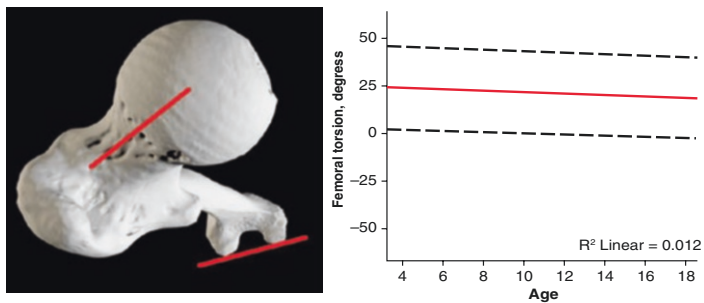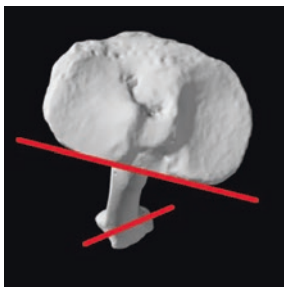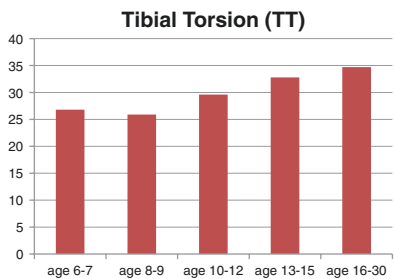
FIGURE 26 Adapted from Szuper et al. [22]

FIGURE 27 Adapted from Gaumétou et al. [28]

- The constraints of the fetus in utero are responsible for tibial deformation, causing a physiological internal TT, which will be from 2° to 10° during the first year of life and from 10° to 20° up to the age of 4 [25].
- Studies performed with EOS imaging have allowed us to reconstruct the evolution of TT in the pediatric age, as described in the values on Fig. 27.
- In adults, the average angle is 23 ± 5.1° [27].

15. Femorotibial Rotation (FTR) [Degrees]: the angle between the posterior bicondylar tangential line of the femur and the posterior bicondylar tangential line of the tibia when projected on an orthogonal plane to the femoral mechanical axis. If this angle is positive, then the tibia is externally rotated relative to the femur.

    To date, there are no published EOS imaging studies on this parameter of the lower limb in children (Fig. 28).

16. Sagittal Femorotibial Angle (SFTA) [Degrees]: angle between the mechanical axis of the femur and the mechanical axis of the tibia in the sagittal plane. The expected value in standing position is 180° (Fig. 29).

    The genu recurvatum is the hyperextension of the knee beyond 180°. The flexion of the knee occurs when the SFTA is less than 180°.

    The flexion/recurvatum is calculated with the formula 180° − STFA. Positive values of SFTA indicate flexion, and negative values indicate genu recurvatum.

    Values of recurvatum between 5° and 15° are considered physiological, and they are found in up to 40% of the population. A recurvatum beyond 15° is usually regarded as pathological [29].
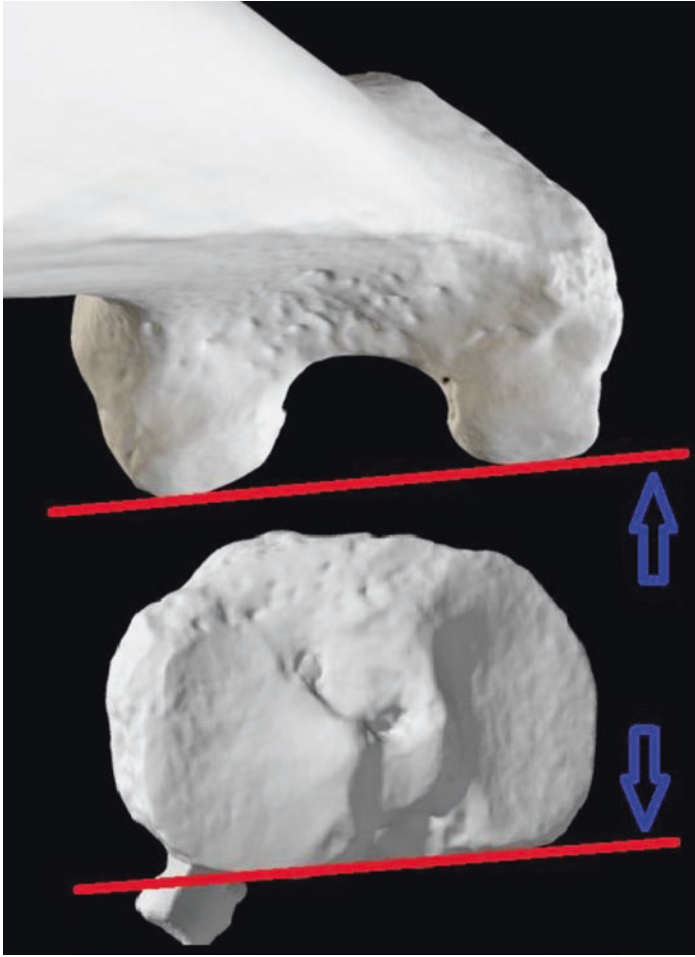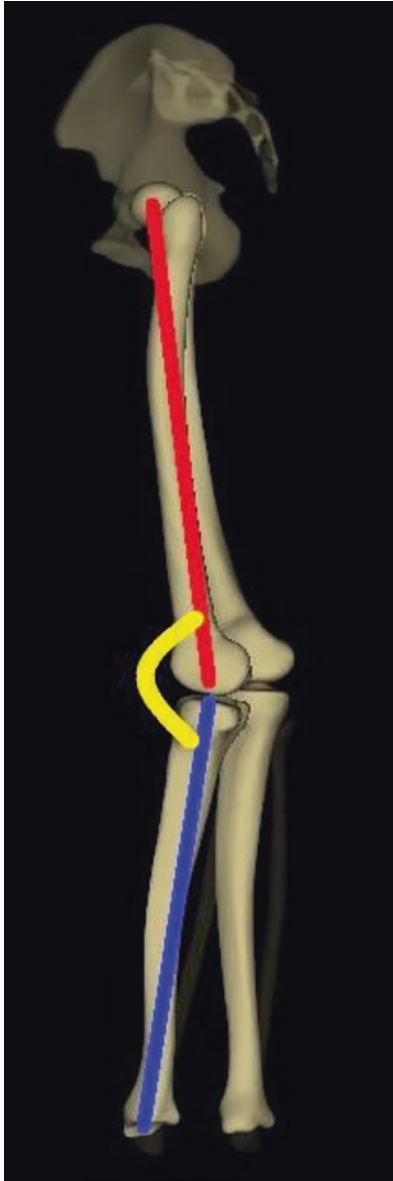
Figure 28 Measurement of femorotibial rotation (FTR)

FIGURE 29 Measurement of the sagittal femorotibial angle (SFTA)

References

1. Wybier M, Bossard P. Musculoskeletal imaging in progress: the EOS imaging system. Joint Bone Spine. 2013;80(3):238–43. Epub 2012 Nov 22. https://doi.org/10.1016/j.jbspin.2012.09.018.

2. McKenna C, Wade R, Faria R, Yang H, Stirk L, Gummerson N, Sculpher M, Woolacott N. EOS 2D/3D X-ray imaging system: a systematic review and economic evaluation. Health Technol Assess. 2012;16(14):1–188. PMID: 22449757; PMCID: PMC4781036. https://doi.org/10.3310/hta16140.

3. Ilharreborde B, Dubousset J, Le Huec JC. Use of EOS imaging for the assessment of scoliosis deformities: application to postoperative 3D quantitative analysis of the trunk. Eur Spine J. 2014;23(Suppl 4):S397–405. Epub 2014 May 9. Erratum in: Eur Spine J. 2014 Jul;23 Suppl 4:S468. PMID: 24811688. https://doi.org/10.1007/s00586-014-3334-7.

4. Melhem E, Assi A, El Rachkidi R, Ghanem I, EOS(®). biplanar X-ray imaging: concept, developments, benefits, and limitations. J Child Orthop. 2016;10(1):1–14. Epub 2016 Feb 16. PMID: 26883033; PMCID: PMC4763151. https://doi.org/10.1007/s11832-016-0713-0.

5. Powell J, Gibly RF, Faulk LW, Carry P, Mayer SW, Selberg CM. Can EOS imaging substitute for conventional radiography in measurement of acetabular morphology in the young dysplastic hip? J Pediatr Orthop. 2020;40(6):294–9.

6. Legaye J, Duval-Beaupère G, Hecquet J, Marty C. Pelvic incidence: a fundamental pelvic parameter for three-dimensional regulation of spinal sagittal curves. Eur Spine J. 1998;7(2):99–103.

7. Bailey JF, Shefi S, Soudack M, Kramer PA, Been E. Development of pelvic incidence and lumbar lordosis in children and adolescents. Anat Rec. 2019;302(12):2132–9.

8. Mac-Thiong JM, Labelle H, Roussouly P. Pediatric sagittal alignment. Eur Spine J. 2011;20(Suppl 5):586–90.

9. Chan CYW. Pelvic obliquity in adolescent idiopathic scoliosis planned for posterior spinal fusion: a preoperative analysis of 311 lower limb axis films. J Orthop Surg. 2019;27(2):2309499019857250.

10. Rousseau MA, Brusson A, Lazennec JY. Assessment of the axial rotation of the pelvis with the EOS® imaging system: intra—and inter-observer reproducibility and accuracy study. Eur J Orthop Surg Traumatol. 2014;24(6):891–5.

11. O'Brien MF, Kuklo TR, Blanke KM, Lenke LG. Spinal deformity study group radiographic measurement manual. Memphis, TN: Medtronic Sofamar Danek; 2008. https://www.oref.org/docs/default-source/default-document-library/sdsg-radiographic-measuremnt-manual.pdf?sfvrsn=2.

12. Kim H, Kim HS, Moon ES, Yoon CS, Chung TS, Song HTS, et al. Scoliosis imaging: what radiologists should know. Radiographics. 2010;30(7):1823–42.

13. Lenke LG, Betz RR, Harms J, Bridwell KH, Clements DH, Lowe TG, et al. Adolescent idiopathic scoliosis: a new classification to determine extent of spinal arthrodesis. J Bone Joint Surg Am. 2001;83(8):1169–81.

14. van den Bogaart M, van Royen B, Haanstra TM, et al. Predictive factors for brace treatment outcome in adolescent idiopathic scoliosis: a best-evidence synthesis. Eur Spine J. 2019;28:511–25. https://doi.org/10.1007/s00586-018-05870-6.

15. Gangnet V, Pomero R, Dumas W, et al. Variability of the spine and pelvis location with respect to the gravity line: a three-dimensional stereoradiographic study using a force platform. Vital Surg Radiol Anat. 2003;25:424–33. https://doi.org/10.1007/s00276-003-0154-6.

16. Legaye J, Duval-Beaupere G. Sagittal plane alignment of the spine and gravity: a radiological and clinical evaluation. Acta Orthop Belg. 2005;71:213–20.

17. Sangondimath G, Mallepally AR, Marathe N, Salimath S, Chhabra HS. Radiographic analysis of the sagittal alignment of spine and pelvis in asymptomatic Indian population. Asian Spine J. 2022;16(1):107–18.

18. Le Huec JC, Thompson W, Moshinaly C, Barrey C, Faundez A. Sagittal balance of the spine. Eur Spine J. 2019;28:1889–905.

19. Mac-Thiong JM, Berthonnaud E, Dimar JR 2nd, Betz RR, Labelle H. Sagittal alignment of the spine and pelvis during growth. Spine (Phila Pa 1976). 2004;29(15):1642–7.

20. Kim JT, Lee DH, Lee HD, Shin HB, Park B, Park S, et al. Validity of the EOS-determined pelvic parameters and orientation with pelvic positional variation: a phantom study. Sci Rep. 2021;11(1):10468.

21. Glaser DA, Doan J, Newton PO. Comparison of 3-dimensional spinal reconstruction accuracy: biplanar radiographs with EOS versus computed tomography. Spine (Phila Pa 1976). 2012;37(16):1391–7.

22. Szuper K, et al. Three-dimensional quantitative analysis of the proximal femur and the pelvis in children and adolescents using an upright biplanar slot-scanning X-ray system. Pediatr Radiol. 2015;45(3):411–21. https://doi.org/10.1007/s00247-014-3146-2.
23. Rampal V, et al. Lower-limb lengths and angles in children older than six years: reliability and reference values by EOS® stereoradiography. Orthop Traumatol Surg Res. 2018;104(3):389–95. https://doi.org/10.1016/j.otsr.2017.10.007.
24. Kinzinger H, Castiaux P. Les vices de torsion des membres inférieurs. Historique, évolution clinique. Acta Orthop Belg. 1977;43:379–470.
25. Chaudier P, Villa V, Neyre P. Traité EM Consulte podologie: anomalie de torsion du squelette. Podologie. 2015:13. https://doi.org/10.1016/S0292-062X(15)60422-6.
26. Gulan G, et al. Femoral neck anteversion: values, development, measurement, common problems. Coll Antropol. 2000;24(2):521–7.
27. Lobenhoffer P, Galla M, Agneskirchner JD. Rotational osteotomies of the femur and the tibia, from: osteotomies around the knee: indications, planning, surgical techniques using plate fixator. Stuttgart, New York.: Distributed by Thieme: Davos: AO Publishing; 2008.
28. Gaumétou E, et al. EOS analysis of lower extremity segmental torsion in children and young adults. Orthop Traumatol Surg Res. 2014;100(1):147–51. https://doi.org/10.1016/j.otsr.2013.09.010.
29. Demey G, Lustig S, Servien E, Neyret P. Genu recurvatum osseux. EMC-Appareil Locomoteur. 2013;5:0246–521.